Hard-Sphere Packing and Icosahedral Assembly in the Formation of Mesoporous Materials

Jiawei Tang,[†] Xufeng Zhou,[†] Dongyuan Zhao,[†] Gao Qing Lu,[§] Jin Zou,[‡] and Chengzhong Yu*,[†]

Contribution from the Department of Chemistry and Shanghai Key Laboratory of Molecular Catalysis and Innovative Materials, Fudan University, Shanghai, 200433, P. R. China, School of Engineering and Centre for Microscopy and Microanalysis, the University of Queensland, QLD 4072, Australia, and ARC Centre for Functional Nanomaterials, the University of Queensland, Brisbane, Australia

Received February 12, 2007; E-mail: czyu@fudan.edu.cn

Abstract: We report the synthesis and characterization of a novel mesoporous material with a face-centered cubic (fcc) symmetry and intrinsic bimodal pores. Moreover, an icosahedral (ICO) mesostructure with both meso- and macroscale 5-fold symmetry is observed. We propose a hard-sphere packing (HSP) mechanism for the formation of mesoporous materials by assuming preformed robust surfactant/silicate composite micelles being hard spheres. In comparison to the conventional liquid crystal templating (LCT) or cooperative self-assembly (CSA) mechanism, our contribution provides an important advancement of knowledge in the study of mesostructured materials.

Introduction

The packing of particles at different length scales (atoms, molecules, and colloid particles) has attracted significant attention in mathematics,[1] physics, chemistry, and material science.[2] It has been recently approved[3] that no other packing of spheres in three dimensions has a density exceeding that of the face-centered cubic (fcc) and the hexagonal close-packed (hcp), although the fcc packing is demonstrated to be more stable than hcp.[4] Mesoporous materials have been assembled by using surfactants as supramolecular templates.[5,6] Despite the different choices of surfactants (cationic,[7] anionic,[7,8] or nonionic[9−12]) and

formation mechanisms, e.g., true liquid crystal templating (LCT),[13] cooperative self-assembly (CSA),[14] etc., the ordered mesostructure may generally find its counterpart in liquid crystal phases. The concept of a simple packing by discrete composite micelles as hard colloidal spheres, however, has not been realized in the formation of mesoporous materials.

Here we demonstrate a hard-sphere packing (HSP) mechanism for the formation of mesoporous materials[5,6] by assuming preformed robust surfactant/silicate composite micelles (Scheme 1A)[15] being hard spheres. In conventional LCT[5,6,13] or CSA[14] mechanisms, the micelles are embedded in the final liquid crystal phase with the inorganic species as the continuous phase; therefore, generally monomodal mesopores are generated after the templates are removed. In great contrast, the assembly of composite colloid hard spheres and the subsequent removal of surfactants leads to a novel fcc mesoporous materials with intrinsic bimodal pores (Scheme 1B). Moreover, an icosahedral (ICO) structure with both meso- and macroscale 5-fold symmetry[16,17] are observed (Scheme 1C). It is anticipated that this novel HSP approach may be further employed to synthesize functional mesoporous materials and monodispersed vesicles with versatile applications.

Experimental Section

The ICO as well as the fcc mesostructured materials were synthesized by using $EO_{132}PO_{50}EO_{132}$ [denoted F108, BASF. EO is poly(ethylene
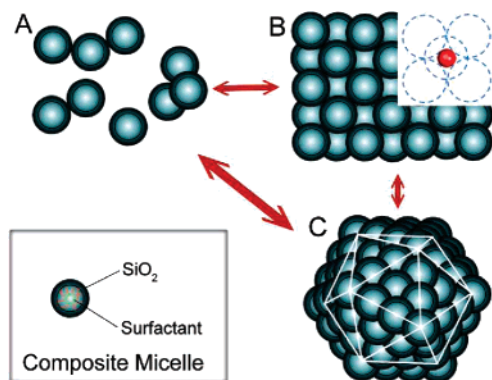
† Fudan University.

‡ School of Engineering and Centre for Microscopy and Microanalysis, the University of Queensland.

§ ARC Centre for Functional Nanomaterials, the University of Queensland.

(1) Hales, T. C.; Sarnak, P.; Pugh, M. C. *Proc. Natl. Acad. Sci. U.S.A.* **2000**, *97* (24), 12963−12964.

(2) Gornostyrev, Y. N.; Katsnelson, M. I.; Trefilov, A. V. *J. Phys.: Condens. Matter* **1997**, *9* (37), 7837−7844.

(3) Hales, T. C. *Discrete Comput. Geom.* **1997**, *17* (1), 1−51.

(4) Woodcock, L. V. *Nature* **1997**, *385* (6612), 141−143.

(5) Kresge, C. T.; Leonowicz, M. E.; Roth, W. J.; Vartuli, J. C.; Beck, J. S. *Nature* **1992**, *359* (6397), 710−712.

(6) Beck, J. S.; Vartuli, J. C.; Roth, W. J.; Leonowicz, M. E.; Kresge, C. T.; Schmitt, K. D.; Chu, C. T. W.; Olson, D. H.; Sheppard, E. W.; McCullen, S. B.; Higgins, J. B.; Schlenker, J. L. *J. Am. Chem. Soc.* **1992**, *114* (27), 10834−10843.

(7) Huo, Q. S.; Margolese, D. I.; Ciesla, U.; Demuth, D. G.; Feng, P. Y.; Gier, T. E.; Sieger, P.; Firouzi, A.; Chmelka, B. F.; Schuth, F.; Stucky, G. D. *Chem. Mater.* **1994**, *6* (8), 1176−1191.

(8) Che, S.; Garcia-Bennett, A. E.; Yokoi, T.; Sakamoto, K.; Kunieda, H.; Terasaki, O.; Tatsumi, T. *Nat. Mater.* **2003**, *2* (12), 801−805.

(9) Tanev, P. T.; Pinnavaia, T. J. *Science* **1995**, *267* (5199), 865−867.

(10) Bagshaw, S. A.; Prouzet, E.; Pinnavaia, T. J. *Science* **1995**, *269* (5228), 1242−1244.

(11) Zhao, D. Y.; Feng, J. L.; Huo, Q. S.; Melosh, N.; Fredrickson, G. H.; Chmelka, B. F.; Stucky, G. D. *Science* **1998**, *279* (5350), 548−552.

(12) Patarin, J.; Lebeau, B.; Zana, R. *Curr. Opin. Colloid Interface Sci.* **2002**, *7* (1−2), 107−115.

(13) Attard, G. S.; Glyde, J. C.; Goltner, C. G. *Nature* **1995**, *378* (6555), 366−368.

(14) Monnier, A.; Schuth, F.; Huo, Q.; Kumar, D.; Margolese, D.; Maxwell, R. S.; Stucky, G. D.; Krishnamurty, M.; Petroff, P.; Firouzi, A.; Janicke, M.; Chmelka, B. F. *Science* **1993**, *261* (5126), 1299−1303.

(15) Huo, Q. S.; Liu, J.; Wang, L. Q.; Jiang, Y. B.; Lambert, T. N.; Fang, E. *J. Am. Chem. Soc.* **2006**, *128* (19), 6447−6453.

(16) Mackay, A. L. *Acta Crystallogr.* **1962**, *15*, 916−918.

(17) Kuo, K. H. *Struct. Chem.* **2002**, *13* (3−4), 221−230.

oxide) and PO represents poly(propylene oxides)] and 1,3,5-trimethylenebenzene (TMB) as cotemplates. For the optimum synthesis condition of mesoporous ICO crystals, the reactant weight ratio was kept at F108/TMB/KCl/TEOS/HCl (2.0 M) = 1.0:1.0:2.5:2.8:30 (g) and the temperature was controlled at 293 K (referred to as the optimum condition hereafter). In a typical synthesis, 1.0 g of F108 and 2.5 g of KCl were dissolved in 30 g of 2.0 M HCl, then 1.0 g of TMB was added into the solution under stirring. After 1 day, 2.8 g of TEOS was added and allowed to react at 293 K under stirring for 15 min, then under the static condition for 1 day. The filtered white precipitates were added into the same concentration of F108/HCl solution and hydrothermally treated at 393 K in an oven for another 1 day. The resultant materials were filtered and dried in air. The surfactants were removed by calcination in air at 823 K for 6 h.

The synthesis conditions, including the ratio of F108, TMB, KCl, tetraethyl orthosilicate (TEOS), HCl, and the synthesis temperature, have been systematically studied. We will focus on the influence of the amount of TEOS and the synthesis temperature upon the final structures in this study (see the Results and Discussion).

X-ray diffraction (XRD) patterns of materials were recorded on a German Bruker D4 X-ray diffractometer with Ni-filtered Cu Kα radiation. Transmission electron microscopy (TEM) images were obtained with a JEOL 2011 microscope operated at 200 kV. For TEM measurements, the samples were prepared by dispersing the powder samples in ethanol, after which they were dispersed and dried on carbon film on a Cu grid. Scanning electron microscopy (SEM) images were obtained on a Philip XL30 microscope operated at 20 kV. Nitrogen adsorption/desorption isotherms were measured at 77 K by using a Micromeritics ASAP Tristar 3000 system. The samples were degassed at 453 K overnight on a vacuum line.

Results and Discussion

SEM investigations of calcined materials synthesized at the optimum condition showed micrometer-sized particles with the majority of them appearing as well-faceted surfaces (Figure 1a). Occasionally, almost perfect icosahedrons with diameters between 1 and 4 μm were observed (Figure 1b). For a rough estimation from SEM observations, the yield of the icosahedrons is less than 1%.
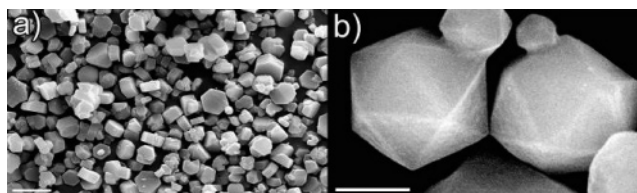

Figure 1. SEM images of mesoporous materials synthesized at 293 K showing (a) the representative morphology and (b) some particles with a near-perfect ICO morphology. The scale bar is 10 and 2 μm in (a) and (b), respectively.

TEM was employed to determine the mesostructure of calcined material synthesized at the optimum condition. In Figure 2a−d are TEM images viewed along different directions. It is of interest to note that Figure 2b shows similar porous patterns to those of fcc mesostructures reported previously;[18,19] whereas Figure 2, parts a, c, and d, shows clearly two sizes of pores, indicating that our mesostructure differs to those reported. Fourier transform of Figure 2a−d is carried out to obtain the diffraction information for different zone axes (Supporting Information Figure S1), from which an fcc mesostructure can be uniquely identified. From the TEM images shown in Figure 2a−d, a lattice parameter of $a \approx 27.0$ nm can be determined for the calcined fcc mesostructure. It is noted that the twin structure is frequently observed along the [110] zone axis (Figure 2d and Figure S1).

The XRD pattern of calcined sample synthesized at the optimum condition is shown in Figure 3, from which an fcc symmetry is also concluded with a space group of *Fm*3*m*, in accordance with our previous reports.[19−21] The cell lattice parameter is calculated to be 27.4 nm. In comparison to highly ordered mesoporous materials with the same symmetry synthesized with other block copolymer templates,[18] the diffraction peak at high angle ($2\theta > 1.5°$) in the XRD pattern of our material is not resolved, indicative of a less-perfect or not pure fcc structure (see Results and Discussion below). Previously, F108 was used as a template to synthesize cubic mesoporous single crystals with a body-centered cubic (bcc) mesostructure in the absence of TMB.[22,23] The utilization of TMB as a cotemplate and the subsequent structural transformation from a bcc to fcc structure is also in accordance with literature reports.[20,24]

The nitrogen sorption analysis was performed to determine the pore structure. Calcined mesoporous silica synthesized at the optimum condition exhibits a type IV isotherm and an H2-type hysteresis loop (Figure 4a), typical of mesoporous materials with a caged pore structure. Figure 4a indicates two sharp capillary condensation steps occurred at high relative pressure range ($P/P_0 = 0.70−0.85$). Accordingly, a bimodal pore size distribution centered at 10.9 and 14.9 nm can be determined

(18) Kleitz, F.; Liu, D. N.; Anilkumar, G. M.; Park, I. S.; Solovyov, L. A.; Shmakov, A. N.; Ryoo, R. *J. Phys. Chem. B* **2003**, *107* (51), 14296−14300.
(19) Fan, J.; Yu, C. Z.; Lei, J.; Zhang, Q.; Li, T. C.; Tu, B.; Zhou, W. Z.; Zhao, D. Y. *J. Am. Chem. Soc.* **2005**, *127* (31), 10794−10795.
(20) Fan, J.; Yu, C. Z.; Gao, T.; Lei, J.; Tian, B. Z.; Wang, L. M.; Luo, Q.; Tu, B.; Zhou, W. Z.; Zhao, D. Y. *Angew. Chem., Int. Ed.* **2003**, *42* (27), 3146−3150.
(21) Yu, T.; Zhang, H.; Yan, X. W.; Chen, Z. X.; Zou, X. D.; Oleynikov, P.; Zhao, D. Y. *J. Phys. Chem. B* **2006**, *110* (43), 21467−21472.
(22) Yu, C. Z.; Fan, J.; Tian, B. Z.; Zhao, D. Y. *Chem. Mater.* **2004**, *16* (5), 889−898.
(23) Yu, C. Z.; Tian, B. Z.; Fan, J.; Stucky, G. D.; Zhao, D. Y. *J. Am. Chem. Soc.* **2002**, *124* (17), 4556−4557.
(24) Zhao, D. Y.; Huo, Q. S.; Feng, J. L.; Chmelka, B. F.; Stucky, G. D. *J. Am. Chem. Soc.* **1998**, *120* (24), 6024−6036.
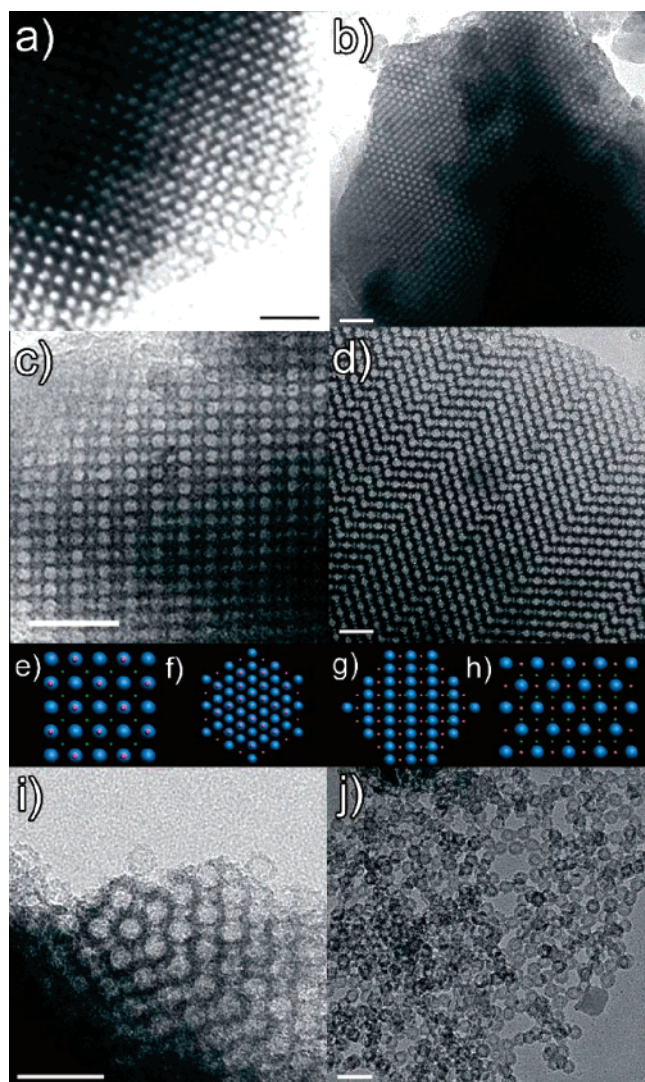
Figure 2. TEM images of the calcined mesoporous materials synthesized at the optimum condition (293 K) with an fcc mesostructure recorded along the (a) [100], (b) [111], (c) [211], and (d) [110] directions. Panels e, f, g, and h are the simulated patterns along the [100], [111], [211], and [110] directions, respectively. The blue spheres represent the mesopores originated from the removal of surfactant micelles; the red and green spheres correspond to the octahedral and the tetrahedral cavity sites in an fcc close packing, respectively. For clarity, the dimensions of the blue, red, and green spheres are not to scale. The TEM image in (i) shows the mesoscale 5-fold symmetry. The TEM image in (j) of materials synthesized at 303 K, while the other reaction conditions are not changed compared to the optimum synthesis, shows monodispersed composite micelles. The scale bar is 50 nm in all images.

by an NLDFT spherical pore model[25] (Figure 4b). On the basis of the nitrogen sorption analysis, the surface area and pore volume for calcined mesoporous materials synthesized at the optimum condition can be measured to be 400 m^2/g and 0.55 cm^3/g, respectively. It is suggested that the larger pores (cages) centered at 14.9 nm with relatively narrower size distribution are generated by the removal of block copolymer templates. However, the smaller pores centered at 10.9 nm with a relatively broader pore size distribution are abnormal, and we will discuss their origin later.

For an fcc structure constructed by a close packing of ideally hard and monodispersed hollow spheres with $a = 27$ nm, an
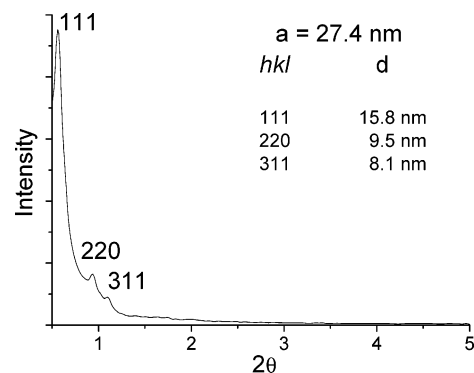
(25) Thommes, M.; Smarsly, B.; Groenewolt, M.; Ravikovitch, P. I.; Neimark, A. V. *Langmuir* **2006**, *22* (2), 756−764.

Figure 3. XRD pattern of calcined mesoporous materials synthesized at the optimum condition. The assignments of the XRD peaks are based on an fcc (*Fm3m*) mesostructure.

o.d. of 19 nm of hollow spheres is required. Since the i.d. of hollow spheres (cages) was determined as 14.9 nm, the wall thickness of 2.1 nm of hollow spheres can be calculated (Supporting Information Figure S2). It is well documented that there are two types of cavities in a simple packed fcc structure: octahedral and tetrahedral sites. The two types of cavities further interconnect into open pores. If these cavities were occupied by smaller inscribed spheres, the diameters for the inscribed spheres in octahedral and tetrahedral sites would be 7.9 and 4.3 nm, respectively. The ratio of the volume of octahedral cavity versus tetrahedral cavity is ∼3.0 (Figure S2). However, it should be taken into account that the pore structures of the octahedral and tetrahedral cavities are complicated, and the actual sizes will be definitely larger than the diameters of the inscribed spheres. We propose that the small pores centered at 10.9 nm should be attributed to the existence of both octahedral and tetrahedral cavities. Because the octahedral cavity possesses larger size and higher volume compared to the tetrahedral cavity, the peak in pore size distribution curve mainly reflects the size of octahedral cavity.

Considering now the fcc packing of hard hollow spheres, projections of the cages and cavities along [100], [111], [211], and [110] directions are schematically given in Figure 2e−h. From our simulation, the cavities cannot be observed from the [111] direction, and the tetrahedral cavity is clearly detectable from the [100] direction (Figure 2a), which are in good accordance with the experimentally viewed images (Figure 2a−d).

Coexisting with the fcc structure, another uniformly arrayed mesostructure with a 5-fold axis was also observed (evidenced in a TEM image shown in Figure 2i) in the sample synthesized at the optimum condition. Very recently, Miyasaka et al. reported the observation of unusual morphologies of mesoporous silica with an fcc symmetry by using short-chain ionic surfactants, including the ICO and decahedral morphologies.[26] On the basis of Figure 2i (5-fold symmetry at the mesoscale) and the SEM evidence that ICO macromorphology is frequently observed, it is proposed that the near-perfect mesostructured icosahedra can be viewed as the multiply twinned fcc structures.[26]

Although the science of ICO has been an interesting topic for 40 years,[27−29] here we show the example of an ICO structure

(26) Miyasaka, K.; Han, L.; Che, S. N.; Terasaki, O. *Angew. Chem., Int. Ed.* **2006**, *45* (39), 6516−6519.
(27) Hubert, H.; Devouard, B.; Garvie, L. A. J.; O'Keeffe, M.; Buseck, P. R.; Petuskey, W. T.; McMillan, P. F. *Nature* **1998**, *391* (6665), 376−378.
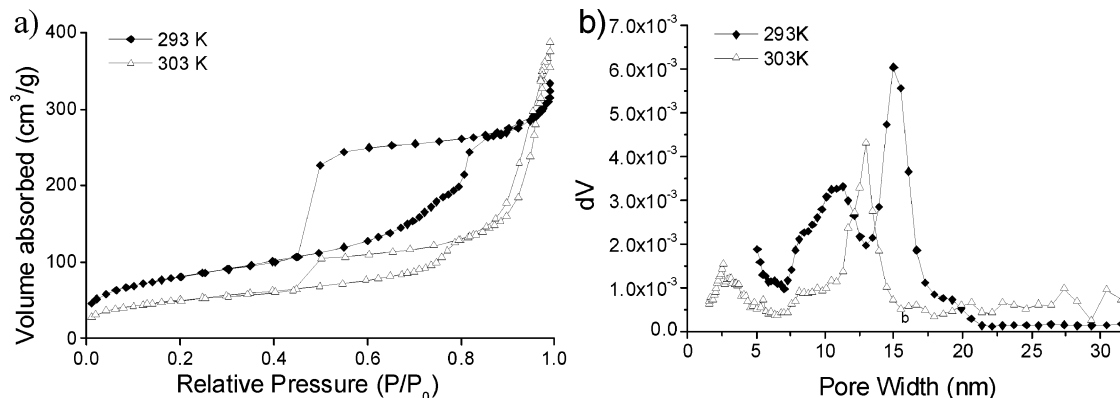
Figure 4. (a) N_2 sorption isotherm and (b) pore size distribution curves calculated from the adsorption branch by the NLDFT method in the spherical model of the calcined mesoporous materials synthesized at the optimum condition (293 K) and another sample synthesized at 303 K while the other reaction conditions are controlled.

packed with infinite equal sized amorphous colloidal spheres, instead of atomic building blocks in former observations. It is also noted that the ICO assembly of definite colloidal spheres has been demonstrated,[30] suggesting that the ICO structure might be a possible candidate during the nucleation stage of colloidal particles (composite micelles in our case). On the other hand, as pointed out by Mackay,[16] the packing density of an ICO packing is smaller than that of an fcc structure; this may explain the fact that the dominant phase observed in our materials is an fcc structure.

In order to prove that the bimodal pore size distribution and the TEM evidence were the results of the packing of the composite micelles, we studied the influence of synthesis parameters upon the final mesostructures. When the synthesis temperature is raised to 303 K while the other synthesis parameters remain unchanged compared to the optimum synthesis conditions, monodispersed siliceous hollow spheres are obtained (Figure 2j). The diameter of the hollow spheres is measured to be 18 nm from TEM images. The N_2 sorption isotherm and the pore size distribution curve of calcined mesoporous material synthesized at 303 K are shown in Figure 4. In comparison with the calcined sample synthesized under the optimum condition at 293 K, the sample obtained at 303 K shows only one pore size distribution peak centered at 13.0 nm (Figure 4b), corresponding to the pore diameter of hollow spheres after removal of surfactant micelles. Moreover, a decrease in the cage size with increased temperature is observed, in accordance with our previous results.[19] The aggregation and random packing of such hollow spheres may lead to interparticle pores evidenced from the capillary condensation step at P/P_0 > 0.9 (Figure 4a). For siliceous materials templated by pluronic EO/PO-type block copolymers, the silica wall contains significant amount of intrawall pores, either in SBA-15-type[31] or SBA-16-type materials.[32] We propose that the hollow cages are accessible to N_2 molecules through such intrawall pores.

When the amount of TEOS is decreased to 1.5−2.0 g at 293

(28) Bachmann, P. K.; Wiechert, D. U. Characterization and Properties of Artificially Grown Diamond. In *Diamond and Diamond-Like Films and Coatings*; Clausing, R. E., Horton, L. L., Angus, J. C., Koidl, P., Eds.; Plenum Press Division of Plenum Publishing Corp: New York, 1991; Vol. 266, pp 677−713.
(29) Hofmeister, H. *Cryst. Res. Technol.* **1998**, *33* (1), 3−25.
(30) Manoharan, V. N.; Elsesser, M. T.; Pine, D. J. *Science* **2003**, *301* (5632), 483−487.
(31) Ravikovitch, P. I.; Neimark, A. V. *J. Phys. Chem. B* **2001**, *105* (29), 6817−6823.
(32) Ravikovitch, P. I.; Neimark, A. V. *Langmuir* **2002**, *18* (5), 1550−1560.
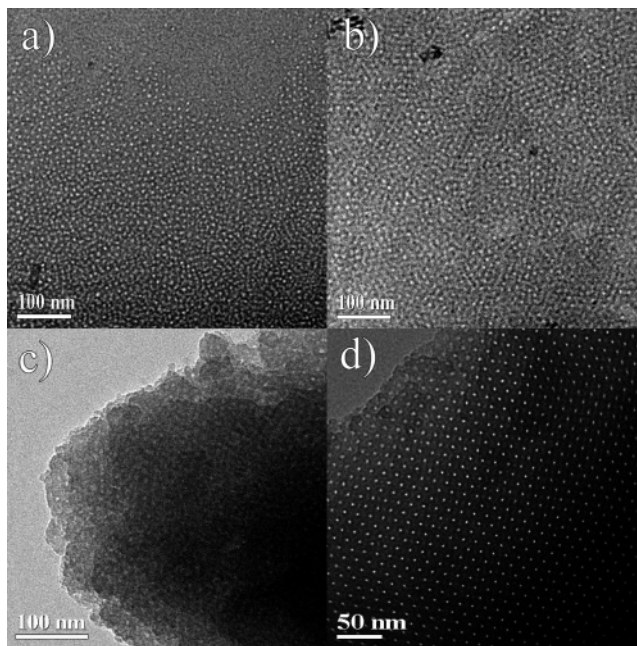
Figure 5. TEM images showing the structural evolution as a function of time (starting after the TEOS is added into the solution) in the optimum synthesis condition when the synthesis temperature is 293 K and the reactant weight ratio is kept at F108/TMB/KCl/TEOS/HCl (2.0 M) = 1.0:1.0:2.5:2.8:30. Panels a, b, c, and d correspond to reaction times of 15 min, 30 min, 6 h, and 12 h, respectively.

K, little precipitates can be observed in the reaction solution. However, monodispersed "hollow spheres" similar to that observed in Figure 2j can be found in TEM observations (Supporting Information Figure S3). These as-synthesized "hollow spheres" should be attributed to "frozen" siliceous composite micelles. Moreover, at the optimum synthesis condition when the amount of TEOS is 2.8 g and the synthesis temperature is 293 K, the structure evolution as a function of time was also studied. Dispersed composite micelles can be directly observed ∼15 min after the addition of TEOS (Figure 5a). Increasing the reaction time may lead to aggregated composite micelles (Figure 5, parts b and c); and the ordered packing of mesostructure is observed after 12 h (Figure 5d).

It should be mentioned that for the calcined sample synthesized at the optimum condition, although the dominant and minor phase is an fcc and ICO structure, respectively (from SEM and TEM observations), little amount of disordered phase similar

Scheme 2. Difference among the LCT (Assembly before Condensation), CSA (Assembly during Condensation), and HSP (Assembly after Condensation) Mechanism for the Formation of Mesoporous Materials[a]
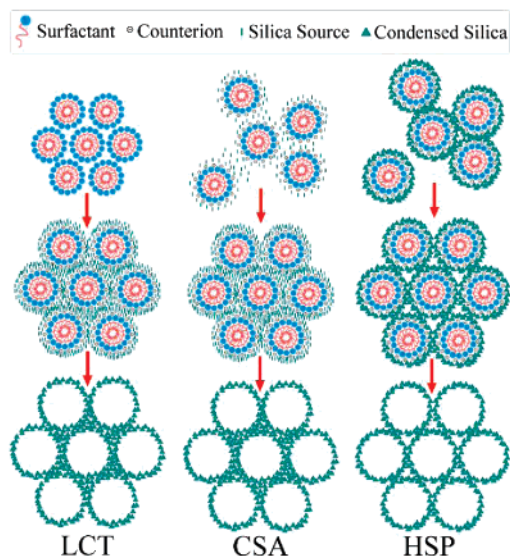
[a] Note that in the final mesoporous materials after the removal of surfactants, an intrinsic bimodal pore size distribution may be generated in the HSP model.

to that shown in Figure 2j is also observed (Supporting Information Figure S4). A distribution among the above three phases in our synthesis system is therefore suggested (Scheme 1) and in accordance with our direct observation of the structural evolution as a function of time. The silicate-coated composite micelles give rise to different structures by tuning the reaction conditions. The fcc phase is dominant at 293 K through the HSP pathway, whereas the spheres without regular packing are favored at a low silica/block copolymer ratio or a relatively high temperature of 303 K. We propose that the fast hydrolysis and condensation rate of siliceous species at the higher temperature may disturb the assembly process of ordered mesostructure; moreover, for the packing process from discrete composite micelles to periodic fcc structure, an entropy loss is accompanied, and thus a decrease in temperature may favor the fcc packing process.

Our proposed HSP mechanism is different from the well-accepted LCT and CSA formation mechanisms (Scheme 2). To be simple, the LCT is an "assembly before condensation" process and the CSA is an "assembly during condensation" process. In either the CSA or the LCT mechanism the micelles are embedded in the final liquid crystal phase with the inorganic species as the continuous phase, which generally leads to monomodal mesopores after the surfactants are removed. In contrast, the HSP pathway is an "assembly after condensation" process. The simple packing of robust composite micelles with condensed walls as hard spheres gives rise to the fcc structure with an intrinsic bimodal pore system (after the removal of surfactant).

Indeed, the HSP phenomenon is quite common in silica spheres, where preformed robust SiO_2 nanospheres usually pack into fcc structures.[33,34] In comparison to the conventional and generally applied LCT and CSA mechanisms, the HSP in the formation of mesostructured materials is relatively limited. The formation of spherical composite micelles, similar to that proposed by Miyasaka et al.,[26] is a precondition in a successful HSP process. Moreover, to apply the HSP mechanism to obtain ordered mesoporous materials with intrinsic bimodal pores, the inorganic wall of spherical composite micelles should be relatively robust, which may behave just like silica spheres.[33,34] In addition, the siliceous species in solutions during the synthesis may also influence the packing of preformed spheres. In our experiments, it is found that the formation of the fcc packing with bimodal pores is achieved when the amount of TEOS is 2.8 g. Less or higher amount of silica source than the optimum condition leads to the monodispersed composite micelles (Figure 2j) or mesoporous materials with monomodel pores (data not shown), respectively.

Conclusions

Novel mesoporous materials with fcc symmetry and intrinsic bimodal pores have been synthesized and well characterized. An ICO mesostructure with both meso- and macroscale 5-fold symmetry is also observed. We propose an HSP mechanism for the formation of mesoporous materials, in which the spherical and monodispersed composite micelles with relatively condensed inorganic walls are used as the building blocks to construct the fcc packing. After removing surfactants, the cages within the composite micelles and the cavity within the fcc stacking give rise to intrinsic bimodal pore structures. The proposed HSP mechanism is an important supplement in understanding the formation mechanism of mesostructured materials. Moreover, with this mechanism, hollow siliceous nanospheres can be easily synthesized, which are good candidates for nanomedicine applications.[15]

Supporting Information Available: The Fourier transformed electron diffraction patterns, additional TEM images, and the calculation process. This material is available free of charge via the Internet at http://pubs.acs.org.

JA070999R

(33) Miguez, H.; Meseguer, F.; Lopez, C.; Mifsud, A.; Moya, J. S.; Vazquez, L. *Langmuir* **1997**, *13* (23), 6009−6011.
(34) Yokoi, T.; Sakamoto, Y.; Terasaki, O.; Kubota, Y.; Okubo, T.; Tatsumi, T. *J. Am. Chem. Soc.* **2006**, *128* (42), 13664−13665.